CHEMISTRY OF MATERIALS

pubs.acs.org/cm

Article

Anisotropic Growth of Silver Nanocubes: The Role of Bromide Adsorption and Hydrophilic Polymers

Heng Xu, Spencer Hao, and Benjamin J. Wiley*

Cite This: *Chem. Mater.* 2023, 35, 7196−7207

Read Online

ACCESS | Metrics & More | Article Recommendations | Supporting Information

ABSTRACT: The application of capping agents to modulate the colloidal synthesis of metal nanocrystals offers an effective avenue for shape control, but the roles of such agents are not yet completely understood. This study uses seed-mediated growth, single-crystal electrochemistry, and surface-enhanced Raman spectroscopy (SERS) to illuminate the roles of polyvinylpyrrolidone (PVP) and bromide (Br^-) in the anisotropic growth of Ag nanocubes. Synthetic results show that Ag nanocubes only form in the presence of both PVP and sufficiently high concentrations of Br^-. Truncated octahedra form in the presence of PVP, and truncated cubes form in the presence of Br^- alone. Electrochemical measurements indicate that elevated concentrations of Br^- consistently passivate Ag(100) facets more than Ag(111) facets regardless of the presence of PVP. The critical condition for the growth of cubes, however, materializes only when both PVP and Br^- are present, which sufficiently suppresses atomic deposition to Ag(100) relative to Ag(111). SERS measurements show that high concentrations of Br^- displace PVP from Ag(100) and Ag(111), but electrochemical measurements suggest PVP acts as a strong passivator under such conditions. We propose that the chemisorption of Br^- beneath a physisorbed layer of PVP creates a unique condition for the growth of Ag nanocubes. Furthermore, our investigation points to a generalizable adsorption structure for the synthesis of {100}-faceted Ag nanocrystals, where Br^- adsorption under other hydrophilic polymers can similarly guide the formation of Ag nanocubes. This study enhances our understanding of the synergistic roles of Br^- and hydrophilic polymers in the controlled morphogenesis of Ag nanocrystals.

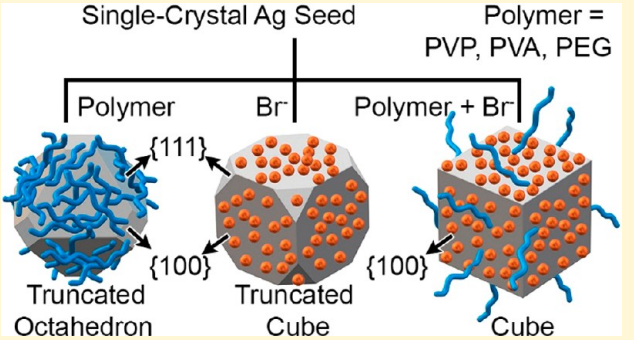

INTRODUCTION

Shape-controlled synthesis of metal nanocrystals offers a pathway to regulate their optical, catalytic, and biological properties.[1−8] This approach typically involves the use of capping agents, which selectively bind to specific facets to influence the atomic deposition rate or surface energy, thereby yielding nanocrystals with different aspect ratios or bounded by distinct facets.[9−13] The unique ability of capping agents to drive anisotropic growth makes a deep understanding of their roles essential for synthesizing metal nanomaterials with the desired shapes and properties. Often, these roles are inferred from the shape of the product synthesized. For example, citrate is considered as a capping agent for Ag(111) because shapes primarily bounded by the {111} facets, such as nanoplates and octahedra, are usually synthesized in the presence of citrate.[14−16]

Conversely, bromide (Br^-) serves as a frequently employed capping agent for synthesizing {100}-enclosed silver (Ag) nanocrystals, such as nanocubes,[17−19] nanowires,[20−24] nanorods,[25] nanobars,[26] and right bipyramids.[27] In these syntheses, Br^- is always added with other organic additives, including polyvinylpyrrolidone (PVP),[26] cetyltrimethylammonium (CTA^+),[17,18] 5-chloro-2-thienylmagnesium,[20] and 6-chlorohexylzinc.[21] The presence of Br^- alone has not produced well-defined shapes, suggesting that the facet-selective growth of these nanocrystals could be attributed to the coadsorption of Br^- with other species. While many {100}-faceted Ag nanostructures can be synthesized with Cl^- as a capping agent, Br^- is especially useful in the synthesis of ultrafine nanostructures that are hard to synthesize with Cl^-, such as sub-20 nm Ag nanocubes[19] and Ag nanowires with diameters of 13−20 nm.[20,22−24] A prevailing hypothesis for the role of Br^- in the formation of sub-20 nm nanostructures is Br^- can strongly passivate Ag(100) to limit the growth along the ⟨100⟩ direction.[24] However, this hypothesis remains largely unverified.

Counter to this hypothesis is the formation of Ag nanoplates predominantly enclosed by {111} facets in the presence of

Received: June 14, 2023
Revised: August 12, 2023
Published: August 18, 2023

cetyltrimethylammonium bromide (CTAB).[28,29] Experiments separating the roles of Br^- from CTA^+ reveal that Br^- is crucial for the growth of Ag nanoplates; replacing CTAB with cetyltrimethylammonium chloride (CTAC) or cetyltrimethylammonium hydroxide (CTAOH) inhibits nanoplate formation.[28] This evidence suggests that Br^- may selectively cap Ag(111) under certain conditions. Yet, in the absence of organic additives protection, such as CTA^+ and 16-mercaptohexadecanoic acid (MHA), Br^- can etch Ag nanoplates into nanodisks.[30,31] These findings underscore the complex role of Br^- and emphasize its study in the context of organic additives.

In this investigation, we integrate seed-mediated growth, single-crystal electrochemistry, and surface-enhanced Raman scattering (SERS) to probe the roles of Br^- in conjunction with PVP with water as the solvent. Synthetic results indicate that Br^- is a weak Ag (100) capping agent in the absence of PVP, but a strong Ag(100) capping agent in the presence of PVP. Electrochemical results show that while Br^- alone can passivate Ag(100) more effectively than Ag(111), the facet selectivity of the passivation is insufficient to produce nanocubes. However, when 60 μM Br^- is introduced alongside 30 mM PVP, the rate of atomic addition to both Ag(100) and Ag(111) reduces and the relative rate of addition to Ag(100) decreases sufficiently to enable nanocube formation. SERS spectra suggest that the presence of 60 μM Br^- displaces most PVP from the Ag surface. In contrast, electrochemical studies indicate that PVP remains physically adsorbed over the chemically adsorbed Br^- adlayer, inhibiting the mass transport of ascorbic acid.

Further synthetic trials demonstrate that adsorption of Br^- with hydrophilic polymers such as poly(vinyl alcohol) (PVA) and poly(ethylene glycol) (PEG) also promotes the growth of Ag nanocubes. This provides evidence of the facet-selective role of Br^- and the non-facet-selective passivating role of hydrophilic polymers. Our study, therefore, presents an innovative approach, leveraging seed-mediated growth, electrochemistry, and SERS to broaden the understanding of the roles of bromide and hydrophilic polymer adsorption in shape-controlled nanocrystal synthesis.

EXPERIMENTAL SECTION

Materials. Silver trifluoroacetate (CF_3COOAg, 98%), L-ascorbic acid (AA, 99%), sodium trifluoroacetate (CF_3COONa, 98%), trifluoroacetic acid (CF_3COOH, 99%), polyvinylpyrrolidone (PVP, MW = 29000 and 55000), sodium citrate dihydrate ($Na_3CA{\cdot}2H_2O$, 99%), benzene-1,4-dithiol (1,4-BDT), dithizone, sodium bromide (NaBr, 99.5%), poly(vinyl alcohol) (PVA, MW = 89000−98000), poly(ethylene glycol) (PEG, MW = 35000), and polyacrylamide (PAM, MW = 40000) were obtained from Sigma-Aldrich. Ethylene glycol (99%) was obtained from J.T. Baker or VWR Chemicals BDH. Acetone and ethanol were obtained from VWR Chemicals BDH. Silver nitrate ($AgNO_3$) and sodium chloride (NaCl) were obtained from Fisher Chemical. Sodium hydroxide (NaOH) was obtained from an EMD Millipore. Ammonium hydroxide (NH_4OH, 50%) and dimethyl sulfoxide (DMSO) were obtained from Beantown Chemical. Hydrochloric acid (HCl, 37%) was obtained from Acros Organics. Chromium(VI) oxide (CrO_3, 99%) was obtained from Alfa Aesar. All of the chemicals were used without further purification.

A silver−silver sulfate reference electrode (saturated K_2SO_4) was purchased from BASi Research Products. A platinum counter electrode was purchased from CH Instruments. Single-crystal silver electrodes were made from single-crystal silver disks (3.0 mm in diameter) purchased from Princeton Scientific based on a previous method.[32]

Synthesis of Truncated Silver Nanocubes as Single-Crystal Seeds. The synthesis of truncated silver nanocubes was based on a previous method with modifications.[32,33] First, 5.00 mL of ethylene glycol (VWR Semi grade or J.T. Baker) was added to a 250 mL double-neck flask preheated at 160 °C with a 20 cm condenser. A light nitrogen gas flow was applied above the solution for 10 min, followed by heating for another 50 min. After this, 2.86 mL of a solution containing 94.00 mM $AgNO_3$ in EG and 2.86 mL of a solution containing 144.0 mM PVP (MW = 55000) and 0.22 mM NaCl in EG were simultaneously added to the flask dropwise within 6 min. The reaction solution turned yellow immediately after the addition of the two solutions and gradually turned clear within 1 h. The reaction solution turned light yellow again at about 4 h and gradually deepened during the next 12 h. At 16 h, the reaction solution turned dark brown, gradually became greenish, and finally turned ochre at 17 h, indicating the reaction was completed. The exact completion time of the reaction can vary between 15 and 21 h. The reaction was quenched in an ice−water bath, 22.00 mL of acetone was added to the reaction solution, and this mixture was centrifuged at 2000*g* for 30 min. The precipitate was washed with 10.00 mL of deionized water three additional times before it was dispersed in 5 mL of deionized water. The single-crystal seeds synthesized in ethylene glycol (J.T. Baker) can be directly used, while the ones synthesized in ethylene glycol (VWR Semi grade) contain some large particles. To purify the single-crystal seeds from large particle impurities, 1 mL of the as-prepared seed solution was diluted to 50 mL and filtered with a 200 nm filter membrane (Whatman). The filtered solution was centrifuged, and the precipitate was washed with 10.00 mL of deionized water before the purified single-crystal seeds were dispersed in 5 mL of deionized water.

Seed-Mediated Growth. The seed-mediated growth was performed with water as the solvent. For a typical synthesis with 30 mM PVP (MW = 29000) and 60 μM Br^-, 2 mL of a 2.4 mM ascorbic acid solution, 1 mL of an 11.88 mM sodium trifluoroacetate solution, 1 mL of a 1.92 mM trifluoroacetic acid solution, 1 mL of a 360 mM PVP (MW = 29000) solution, 0.5 mL of a 1.44 mM NaBr solution, 2.44 mL of water, and 0.06 mL of seeds (or 2.37 mL of water and 0.13 mL of purified seeds) were first mixed. Following this, 4 mL of a 0.6 mM silver trifluoroacetate solution was added. The solution was stirred for 15 min and then centrifuged at 10000 rpm for 4 min. The precipitate was washed with 10 mL of deionized water four times and centrifuged at 10000 rpm for 4 min. The product was dispersed in 0.5 mL of deionized water for imaging. Syntheses with other Br^- concentrations or polymers were performed in the same manner except the concentrations of NaBr were changed or different polymers were used.

Scanning Electron Microscopy (SEM). SEM images were obtained with an Apreo S scanning electron microscope (ThermoFisher Scientific). The single-crystal seeds were imaged at an accelerating voltage of 2.0 kV and a beam current of 25 pA. Other samples were imaged at an accelerating voltage of 10.0 kV and a beam current of 50 pA. The samples were prepared by dropping 2−10 μL of the sample solutions on a piece of silicon followed by drying in air.

Electrochemical Measurements. The single-crystal silver electrodes were prepared based on a modified etching method.[32] The Ag(100) and Ag(111) electrodes (3 mm in diameter) were first mechanically polished with alumina powder (0.3 μm) until they appeared to have mirror-like surfaces. Then, each of the electrodes was dipped in three stirred solutions: (1) chromium trioxide (0.15 M) and hydrochloric acid (0.1 M) for 1 min, (2) 50% ammonium hydroxide for 5 min, and (3) trifluoroacetic acid (4 M) for 2 min. The electrodes were thoroughly rinsed with a flow of deionized water and dried with a flow of nitrogen gas after etching in each solution. Note that chromium trioxide is highly toxic, while the acids and base used in the etching solutions are volatile and corrosive. These experiments must be performed in a fume hood with proper protection.

The facet selectivity of PVP and Br^- was measured by performing linear sweep voltammetry (LSV) in the seed-mediated growth solution without the addition of the seeds. The seed-mediated growth occurred too quickly for electrochemical analysis of the mixed

https://doi.org/10.1021/acs.chemmater.3c01485
Chem. Mater. 2023, 35, 7196−7207

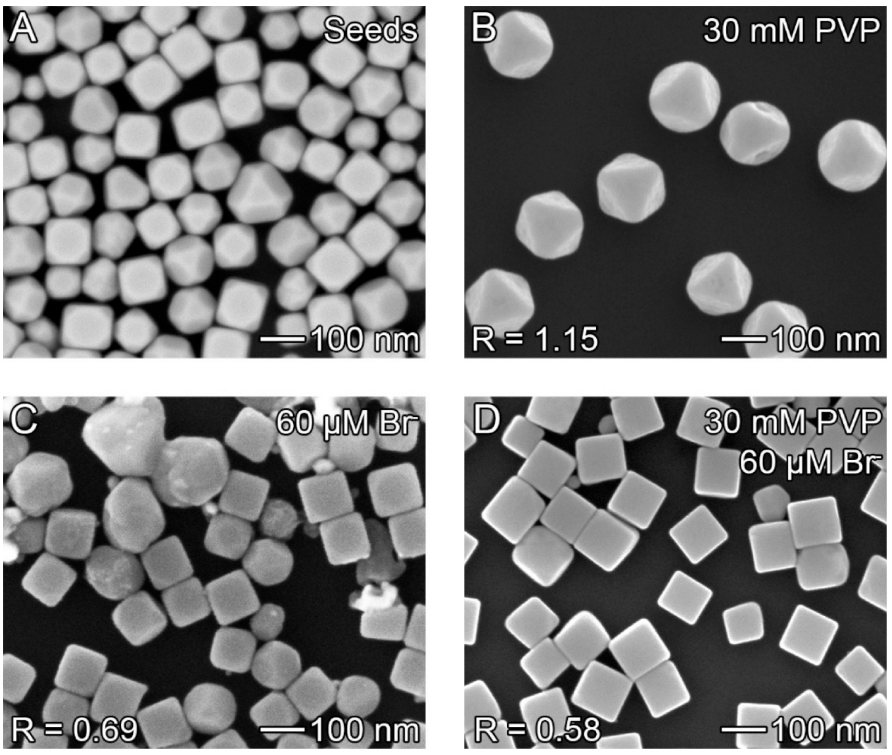

Figure 1. (A) SEM image of the single-crystal seeds. (B–D) Results from growth of the single-crystal seeds with (B) 30 mM PVP, (C) 60 μM Br^-, and (D) 30 mM PVP and 60 μM Br^-. All seed-mediated growth was performed by using 0.2 mM CF_3COOAg as a silver precursor and 0.4 mM AA as a reducing agent.

reaction solution (the reaction was complete in 15 min), so the rates of silver ion reduction and ascorbic acid oxidation at the mixed potential were analyzed separately, i.e., in solutions containing no ascorbic acid and no silver ions, respectively. LSV was performed from −0.28 to −0.03 V at a rate of 5 mV/s with one polished single-crystal silver electrode as a working electrode, an Hg/Hg_2SO_4 electrode (saturated K_2SO_4) as a reference electrode, and a platinum wire as a counter electrode. Each solution was stirred for 2 min before the electrodes were placed into the solution, and the electrodes were held in the solution for 2 min before starting the LSV scan. The solutions were constantly stirred at 500 rpm during the measurement.

Synthesis of Ag Nanocubes. Ag nanocubes were grown from the single-crystal seeds. 76 mL of DI water, 4 mL of a 24 mM AA solution, 20 mL of a 11.88 mM CF_3COONa solution, 20 mL of a 1.92 mM CF_3COOH solution, 20 mL of a 360 mM PVP solution, 1.2 mL of the single-crystal seed solution, and 20 mL of a 72 μM NaCl were mixed in a 300 mL beaker under stirring. Following this, 80 mL of a 0.6 mM CF_3COOAg solution was added. The solution was stirred 1 min before the beaker was sealed by parafilm. The solution was stirred for another 19 min before the product was centrifuged and washed with DI water four times. The product was dispersed in 2 mL of DI water for future use.

Synthesis of Ag Octahedra. Ag octahedra were grown from the single-crystal seeds. 123.2 mL of water, 4 mL of a 24 mM AA solution, 4 mL of a 54 mM Na_3CA solution, 7.6 mL of a 60 mM CF_3COOH solution, 20 mL of a 360 mM PVP solution, and 1.2 mL of the single-crystal seed solution were mixed in a 300 mL beaker under stirring. Following this, 80 mL of a 0.6 mM CF_3COOAg solution was added. The solution was stirred 1 min before the beaker was sealed by parafilm. The solution was stirred for another 12 min before the product was centrifuged and washed with DI water four times. The product was dispersed in 2 mL of DI water for future use.

Quantification of Ag Nanocube and Ag Octahedron Concentrations. The concentrations of Ag nanocubes and Ag octahedra were quantified by a dithizone-based colorimetric assay.[34] Coordination of dithizone to Ag^+ leads to a decrease in light absorption at 618 nm, making it possible to quantify the concentration of Ag^+ based on the UV–vis spectra of mixed solutions of dithizone and Ag^+ analytes.

To convert Ag nanocrystals to Ag^+, 20 μL of a Ag nanocube or Ag octahedron solution and 20 μL of 70% HNO_3 were first mixed. After the nanocrystals dissolved, 0.96 mL of DI water was added, and the solution was thoroughly mixed. This solution was used as the analyte solution for Ag nanocube and octahedron concentration measurements.

The UV–vis spectra of dithizone at different Ag^+ concentrations were first collected. A series of $AgNO_3$ solutions (0.0, 0.4, 0.6, 0.8, 1.0, and 1.2 mM $AgNO_3$ in 1.4% HNO_3) were used as standard solutions. Each time, 0.05 mL of one of the standard solutions was first mixed with 1.2 mL of DMSO for 30 s. After this, 0.2 mL of a 0.5 mM dithizone DMSO solution was added. The solution was thoroughly mixed, and the UV–vis spectrum was collected (Agilent Cary 6000i). A standard curve was generated based on the absorbance at 618 nm at different Br^- concentrations.

To measure the concentrations of Ag nanocubes and Ag octahedra, 0.05 mL of an analyte solution of Ag nanocubes or Ag octahedra was first mixed with 1.2 mL of DMSO for 30 s. After this, 0.2 mL of a 0.5 mM dithizone DMSO solution was added. The solution was thoroughly mixed, and the UV–vis spectrum was collected. The absorbance at 618 nm was used to calculate the concentrations of Ag nanocubes (32.45 ± 0.14 mM, 3.61×10^{11} particles/mL) and Ag octahedra (29.05 ± 0.35 mM, 3.98×10^{11} particles/mL). The Ag nanocubes and Ag octahedra were diluted to 3.6×10^{11} particles/mL to be used as the stock solutions.

Surface-Enhanced Raman Spectroscopy (SERS). Raman spectra were collected with a Raman microscope (Horiba Jobin Yvon LabRam ARAMIS). Sample solutions were prepared by mixing 20 μL of Ag nanocube or octahedral stock solution (3.6×10^{11} particles/mL), 20 μL of a 90 mM PVP solution, and 20 μL of water or NaBr solutions of different concentrations. In each measurement, 50 μL of a sample solution was dropped on a precleaned glass slide, and a 442 nm laser was focused through a 50× objective lens on a plane that was slightly below the liquid surface, with a 50 μm laser spot appearing on the liquid surface. A 2400 grating, a 100% filter, and a

https://doi.org/10.1021/acs.chemmater.3c01485
Chem. Mater. 2023, 35, 7196–7207

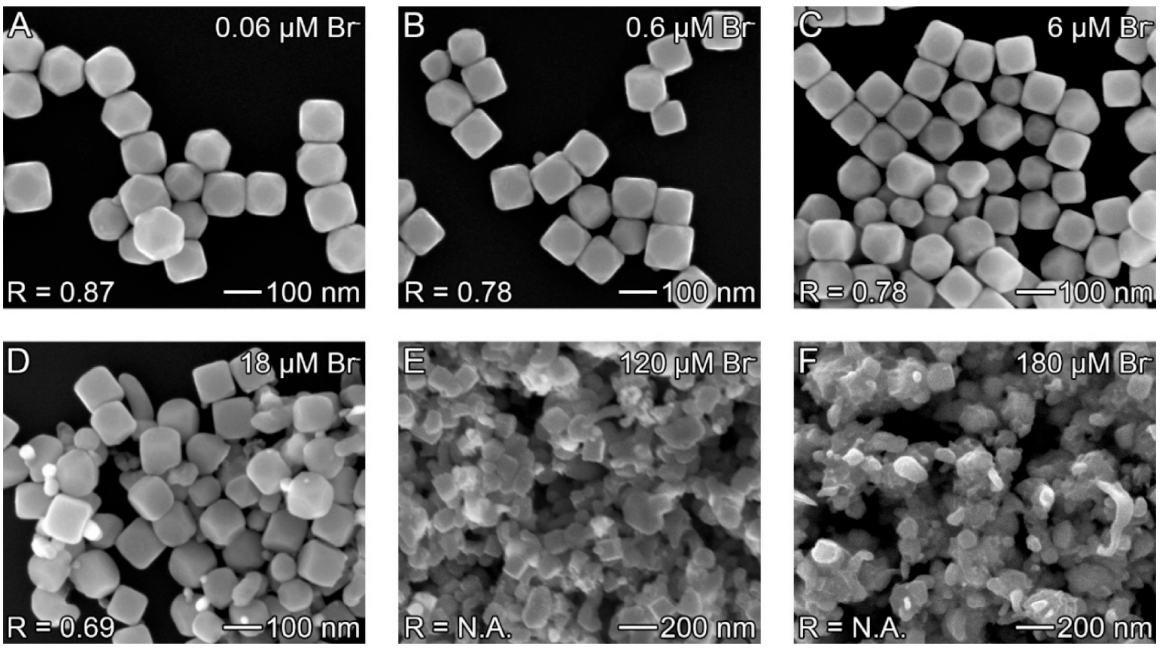

Figure 2. SEM images of silver nanocrystals grown from single-crystal seeds in the presence of no PVP and different concentrations of Br^-: (A) 0.06, (B) 0.6, (C) 6, (D) 18, (E) 120, and (F) 180 μM. All seed-mediated growth was performed by using 0.2 mM CF_3COOAg as a silver precursor and 0.4 mM AA as a reducing agent.

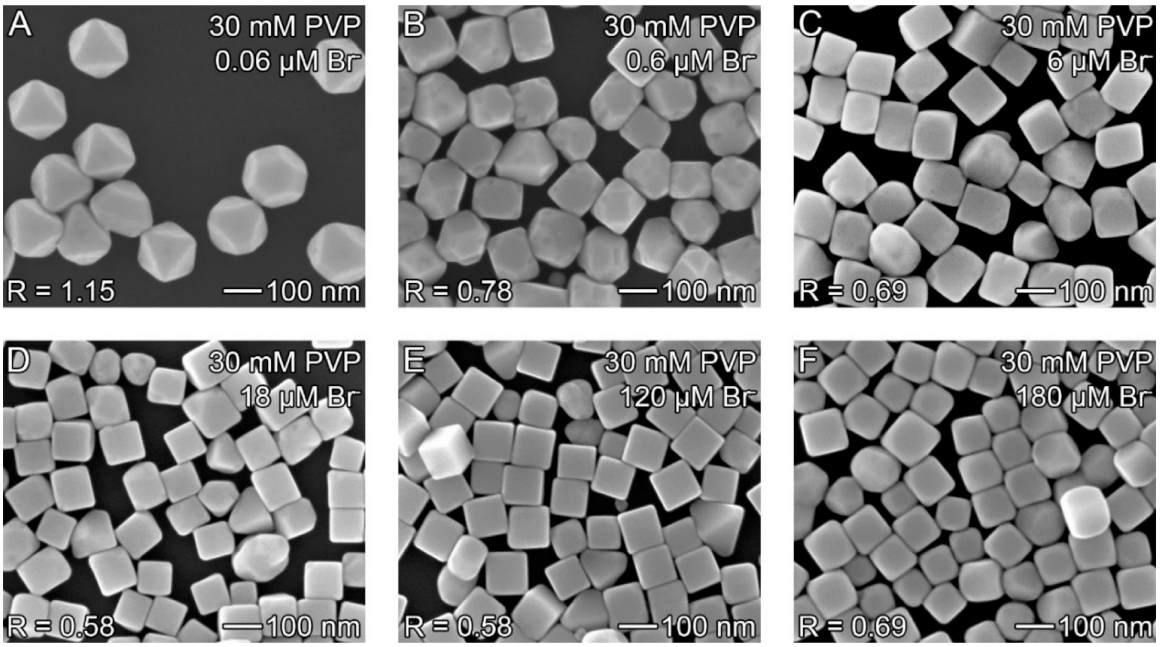

Figure 3. SEM images of silver nanocrystals grown from single-crystal seeds in the presence of 30 mM PVP and different concentrations of Br^-: (A) 0.06, (B) 0.6, (C) 6, (D) 18, (E) 120, and (F) 180 μM. All seed-mediated growth was performed by using 0.2 mM CF_3COOAg as a silver precursor and 0.4 mM AA as a reducing agent.

400 slit were used. Each acquisition lasted for 5 s, and 10 acquisitions were accumulated to generate one Raman spectrum. Each sample was measured three times.

Samples containing 1,4-BDT were measured in the same manner. The Raman spectrum of 100 mM 1,4-BDT was directly measured from 50 μL of an aqueous solution containing 100 mM 1,4-BDT and 12 M NaOH. To measure the SERS spectra of 1,4-BDT on Ag octahedra or Ag cubes, 50 μL of Ag octahedron or Ag cube stock solutions was first centrifuged and dispersed in 150 μL of 1 mM 1,4-BDT in ethanol. After 3 h, the solution was centrifuged and washed with 150 μL of ethanol before 1,4-BDT-functionalized Ag octahedra or Ag cubes were dispersed to 1.2×10^{11} particles/mL in 150 μL of DI water for SERS measurements. The SERS spectra were measured from 50 μL of as-prepared solutions.

RESULTS AND DISCUSSION

Effect of Br^- on the Facet Selective Growth of Ag Nanocrystals. The seed-mediated growth of single-crystal seeds was employed to investigate the influence of Br^- on Ag nanocrystal growth. Ascorbic acid (AA) functioned as a reducing agent that converts Ag^+ ions to Ag atoms, which are

https://doi.org/10.1021/acs.chemmater.3c01485
Chem. Mater. 2023, 35, 7196−7207

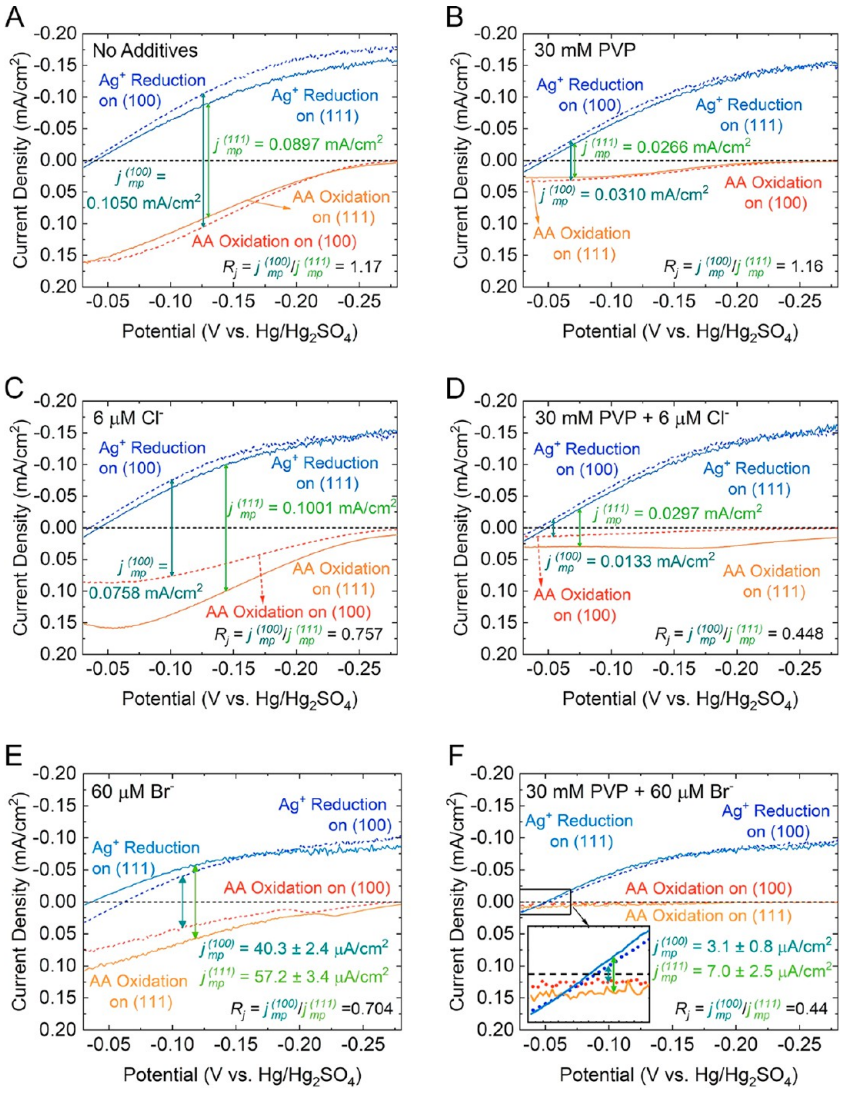

Figure 4. LSVs for Ag^+ reduction and AA oxidation half-reactions on Ag(100) and Ag(111) electrodes in the presence of different capping agents: (A) no additives, (B) 30 mM PVP, (C) 6 μM Cl^-, (D) 30 mM PVP and 6 μM Cl^-, (E) 60 μM Br^-, and (F) 30 mM PVP and 60 μM Br^-. Panels A–D were reproduced with permission from ref 37. Copyright 2023 the Royal Society of Chemistry.

deposited onto the seed and contribute to its growth. Given the frequent usage of PVP alongside halides, we also evaluated the impact of Br^- in conjunction with PVP. All of the seed-mediated growth experiments were performed with water as the solvent.

The single-crystal seeds were synthesized with a polyol method and comprised a blend of truncated cubes and cuboctahedra (Figure 1A). The shape into which the single crystal seeds evolve is dependent on the ratio (R) of atomic deposition rate along the ⟨100⟩ direction ($\text{growth}_{\langle 100\rangle}$) and the ⟨111⟩ direction ($\text{growth}_{\langle 111\rangle}$):

$$R = \text{growth}_{\langle 100\rangle}/\text{growth}_{\langle 111\rangle}$$

As R increases from 0.58 to 1.73, the shape of the single-crystal product changes from a cube to an octahedron (Figure S1).[32,35,36] When 30 mM PVP is present, the seeds evolve into truncated octahedra (with an R value of ∼1.15), in line with our prior findings.[37] In the presence of 60 μM Br^-, the product is a mixture of truncated cubes (R = 0.69) and irregular particles (Figure 1C). Some irregular particles are smaller than the size of the seeds, indicating they may form from heterogeneous nucleation or from the etching of the seeds by Br^- as evidenced by the etched half cube (Figure 1C). In the presence of 30 mM PVP and 60 μM Br^-, the seeds grew to form nanocubes with an R of 0.58 (Figure 1D).

Effect of Br^- Concentration. When the Br^- concentration is 0.06 μM, most single-crystal seeds form cuboctahedra with an R of 0.87 (Figure 2A). Given the similarity to the shapes formed without capping agents, we suggest that this low concentration of Br^- does not notably impact facet-selective growth.[32,37] As Br^- concentration rises to 0.6–6 μM, the product becomes a mixture of cuboctahedra (R = 0.87) and truncated cubes (R = 0.69), resulting in an average R value of 0.78 (Figure 2B,C). Upon reaching 18 μM Br^-, the product is a combination of truncated cubes (R = 0.69) and irregular particles (Figure 2D), similar to the situation with 60 μM Br^-. Further increases to 120 and 180 μM Br^- led to the formation of irregular nanoparticles (Figure 2E,F), which exhibit rapid shape changes under the electron beam of the scanning electron microscope (SEM), suggesting a composition inclusive of AgBr.

https://doi.org/10.1021/acs.chemmater.3c01485
Chem. Mater. 2023, 35, 7196–7207

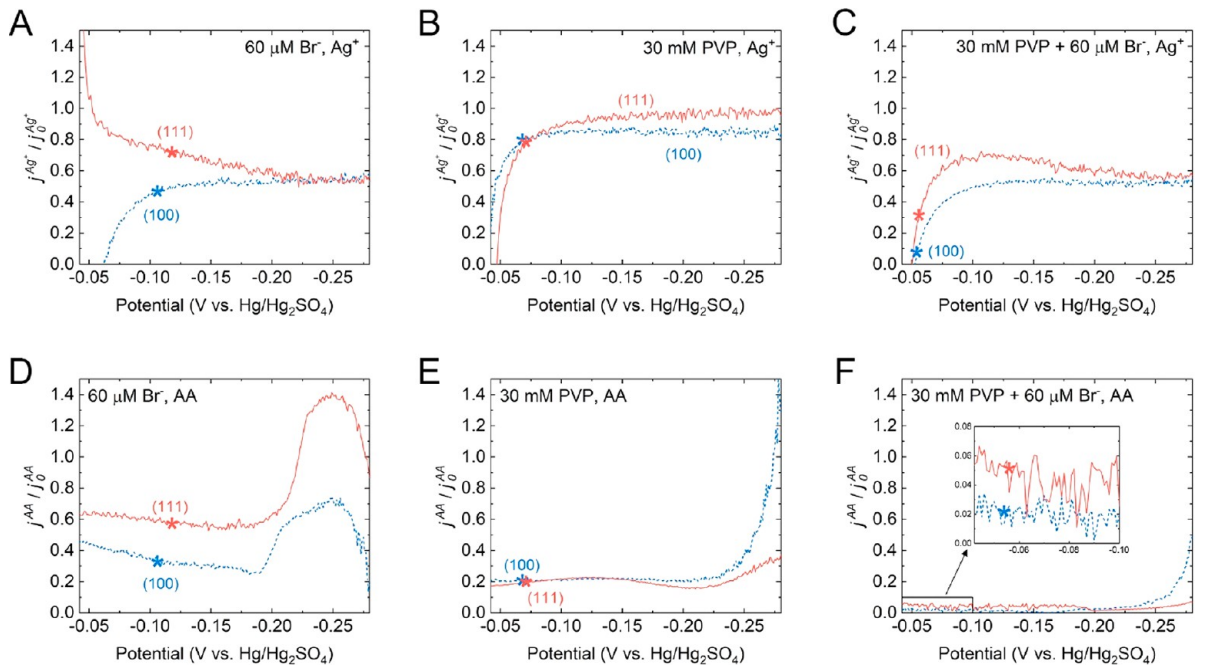

Figure 5. Ratios of half-reaction current densities (j^{AA} or j^{Ag^+}) with capping agents and half-reaction current densities without any capping agents (j_0^{AA} or $j_0^{Ag^+}$). (A) $j^{Ag^+}/j_0^{Ag^+}$ in the presence of 60 μM Br^-. (B) $j^{Ag^+}/j_0^{Ag^+}$ in the presence of 30 mM PVP. (C) $j^{Ag^+}/j_0^{Ag^+}$ in the presence of 30 mM PVP and 60 μM Br^-. (D) j^{AA}/j_0^{AA} in the presence of 60 μM Br^-. (E) j^{AA}/j_0^{AA} in the presence of 30 mM PVP. (F) j^{AA}/j_0^{AA} in the presence of 30 mM PVP and 60 μM Br^-. $*$ indicates the mixed potentials.

We also evaluated the effect of the Br^- concentration in the presence of PVP. When 30 mM PVP and 0.06 μM Br^- are combined, the seeds grow to form truncated octahedra with an R of 1.15 (Figure 3A). The same shape forms with only 30 mM PVP present (Figure 1B), indicating that 0.06 μM Br^- does not significantly influence the seed growth. However, with 30 mM PVP and 0.6 μM Br^-, the seeds evolve into truncated cubes and cuboctahedra (Figure 3B). Notably, the nanocrystals' surface appears uneven, with some elongating along one axis to form truncated nanobars, likely due to the uneven adsorption of Br^- on the crystal facets.[26] As the Br^- concentration increases to 6 or 18 μM, in the presence of 30 mM PVP, the seeds form slightly truncated cubes (Figure 3C,D). When the concentration of Br^- reaches 120 μM alongside 30 mM PVP, sharp-cornered cubes form with few irregular particles (Figure 3E). This is similar to cube formation in the presence of 30 mM PVP and 60 μM Br^-. However, when the Br^- concentration increases to 180 μM in conjunction with PVP, the seeds form truncated cubes with an R of 0.69 (Figure 3F). In this condition, almost no cuboctahedron seeds remain, suggesting continued seed growth despite the high Br^- concentration. The shapes into which the single-crystal seeds evolve under different conditions are summarized in Table S1 for comparison.

Compared with our previous work on the role of PVP and Cl^- in the anisotropic growth of Ag nanocrystals, the seed-mediated growth results show Cl^- and Br^- have similar effects on the anisotropic growth of Ag nanocrystals.[37] In the absence of PVP, 0.6–60 μM either Cl^- or Br^- leads to the growth of truncated cubes. The only difference is 18–60 μM Br^- can cause the formation of irregular particles, while Cl^- does not. In the presence of PVP, the addition of 3–6 μM Cl^- or 60–120 μM Br^- results in cube growth. The requisite halide concentration for cube growth is 10–40 times higher for Br^- than that for Cl^-. Below these necessary halide concentration ranges for cubes, the addition of either Cl^- or Br^- yields intermediate shapes, such as cuboctahedra and truncated cubes. Conversely, above these required halide concentration ranges, the addition of 18 μM Cl^- or 120 μM Br^- promotes the growth of truncated cubes. These findings underscore the significance of halides in regulating the anisotropic growth of silver nanocrystals.

Electrochemical Measurements of the Silver Deposition Rate on Ag(100) and Ag(111). We employed Ag(100) and Ag(111) single-crystal electrodes to ascertain the influence of Br^- on Ag deposition on the {100} and {111} facets. Each single-crystal electrode's surface is covered exclusively by one type of crystallographic plane, either (100) or (111), providing a model for the surface facets of silver nanocrystals. In the seed-mediated growth reaction, Ag^+ ions are reduced by AA, indicating the reaction must happen at a potential where the rate of Ag^+ gaining electrons is equal to the rate of AA losing electrons. This potential, which is known as the mixed potential (E_{mp}), is determined by identifying the potential where the currents for Ag^+ reduction and AA oxidation are equal and opposite. The current density (j_{mp}) at E_{mp} indicates reaction rate.[32] The ratio of j_{mp} between Ag(100) and Ag(111) ($R_j = j_{mp}^{(100)}/j_{mp}^{(100)}$) predicts the shape that will form under the measured condition.

In our prior work, we utilized this method to investigate the effects of PVP and Cl^- on the Ag^+ reduction and AA oxidation half-reactions (Figure 4A–D).[37] The results showed that 30 mM PVP significantly passivates AA oxidation in a non-facet-selective manner (Figure 4B). Moreover, 6 μM Cl^- passivates AA oxidation more on Ag(100) than on Ag(111), but R_j is not small enough for cube growth (Figure 4C). In the presence of both 30 mM PVP and 6 μM Cl^-, the passivation of AA oxidation on Ag(100) exceeds that on Ag(111), and R_j is less

https://doi.org/10.1021/acs.chemmater.3c01485
Chem. Mater. 2023, 35, 7196–7207

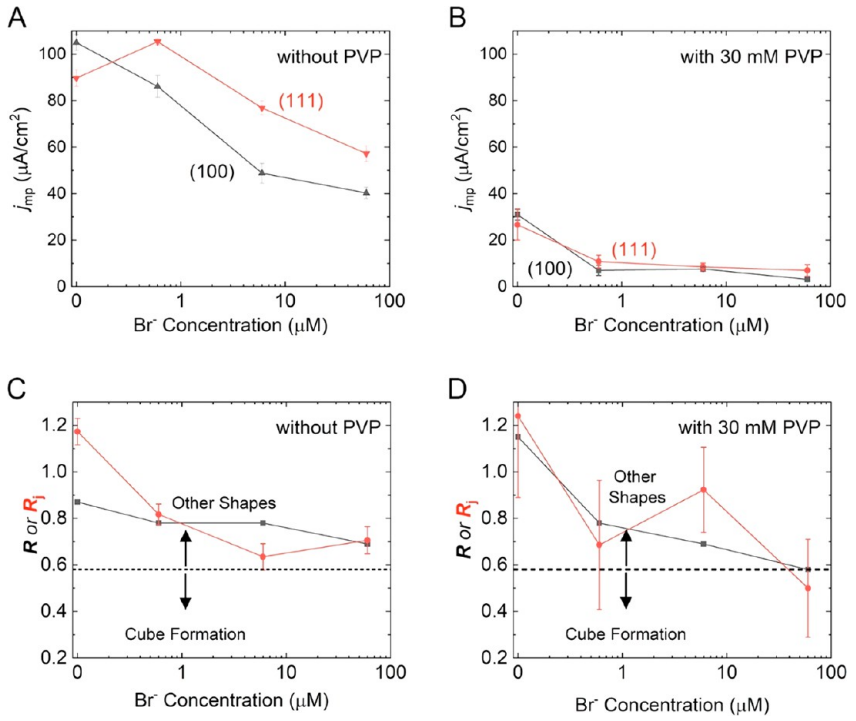

Figure 6. (A) j_{mp} values at different Br^- concentrations. (B) j_{mp} values at different Br^- concentrations in the presence of 30 mM PVP. (C) R and R_j values at different Br^- concentrations in the absence of PVP. (D) R and R_j values at different Br^- concentrations in the presence of 30 mM PVP.

than 0.58, creating a condition for cube growth (Figure 4D). In all of these conditions, the capping agents did not markedly affect Ag^+ reduction, implying that PVP and Cl^- regulate the anisotropic growth of Ag nanocrystals by modulating the AA oxidation rate, which, in turn, limits the rate of Ag^+ reduction.

With 60 μM Br^-, $j_{mp}^{(100)}$ = 40.3 μA/cm^2 and $j_{mp}^{(111)}$ = 57.2 μA/cm^2, giving R_j = 0.704 (Figure 4E). This is congruent with the formation of truncated cubes (R = 0.69) with 60 μM Br^- (Figure 1C). When compared with the condition with no capping agents (Figure 4A), $j_{mp}^{(100)}$ is suppressed by 61.6% and $j_{mp}^{(111)}$ is suppressed by 36.2%.[37] This outcome indicates that 60 μM Br^- is a passivator for both facets, but it passivates Ag(100) more than Ag(111).

When 60 μM Br^- is added with 30 mM PVP, $j_{mp}^{(100)}$ = 3.1 μA/cm^2 and $j_{mp}^{(111)}$ = 7.0 μA/cm^2, giving R_j = 0.44 (Figure 4F). This value is smaller than the R of the nanocubes (0.58), which agrees with the synthetic result (Figure 1D). Compared with the condition of 30 mM PVP (Figure 4B), $j_{mp}^{(100)}$ is further reduced by 90% and $j_{mp}^{(111)}$ is further reduced by 73%.[37] These results demonstrate that the addition of 60 μM Br^- to 30 mM PVP significantly enhances the passivation of both Ag(100) and Ag(111), with a more pronounced effect on Ag(100).

We observed a noteworthy difference in the passivation effects of 60 μM Br^- on Ag(100) compared to Ag(111) near the E_{mp} value (Figure 4E). Surprisingly, this observation contradicts our previous findings, where capping agents, such as citrate, PVP, and Cl^-, exhibited facet-selective passivation only for AA oxidation. This discrepancy suggests that the anisotropic growth of Ag nanocrystals in the presence of Br^- may involve a distinct mechanism.[32,37]

To quantitatively assess the impact of capping agents on the two half-reactions, we utilized the ratios of half-reaction current densities in the presence (j^{AA} or j^{Ag^+}) and absence (j_0^{AA} or $j_0^{Ag^+}$) of capping agents. Lower current density ratios indicate stronger passivation.

In the absence of PVP, 60 μM Br^- exhibited greater passivation on Ag(100) than on Ag(111) near the E_{mp} (Figure 5A,D). However, concerning Ag^+ reduction, Br^- displayed stronger passivation on Ag(100) than on Ag(111) only in the anodic region (−0.05 to −0.20 V vs Hg/Hg_2SO_4), where Ag^+ reduction is limited by activation energy (kinetically limited). In the cathodic region (−0.20 to −0.25 V vs Hg/Hg_2SO_4), where Ag^+ reduction is hindered by mass transfer, Ag^+ reduction was passivated, but the passivation was not facet-selective. This suggests that the reduction of AgBr on Ag(100) is more difficult than that on Ag(111), while the adsorption of Br^- on Ag surfaces does not cause facet-selective mass transfer. With regard to AA oxidation, Br^- exhibited stronger passivation on Ag(100) across the entire measured potential range, indicating that Br^- impedes AA oxidation by creating facet-selective barriers in both energy and mass transfer.

In the presence of 30 mM PVP, the degree of passivation was similar between Ag(100) and Ag(111) for both half-reactions (Figure 5B,E), suggesting that PVP is not facet-selective. However, PVP passivates AA oxidation by 80%, whereas it passivates only Ag^+ reduction by approximately 20%. This indicates that PVP primarily influences the growth of Ag nanocrystals by passivating AA oxidation, which further limits the Ag^+ reduction.

When both 30 mM PVP and 60 μM Br^- were present, both half-reactions exhibited greater passivation on Ag(100) than on Ag(111) near the E_{mp} (Figure 5C,F). The passivation degree for Ag^+ reduction was around 40%, and the passivation curves for Ag^+ reduction under this condition closely resemble those of 60 μM Br^- without PVP (Figure 5A,C), indicating that the passivation of Ag^+ reduction mainly originated from Br^-. For AA oxidation, the degree of passivation exceeds 90% in the presence of 30 mM PVP and 60 μM Br^- (Figure 5F). It is

https://doi.org/10.1021/acs.chemmater.3c01485
Chem. Mater. 2023, 35, 7196−7207

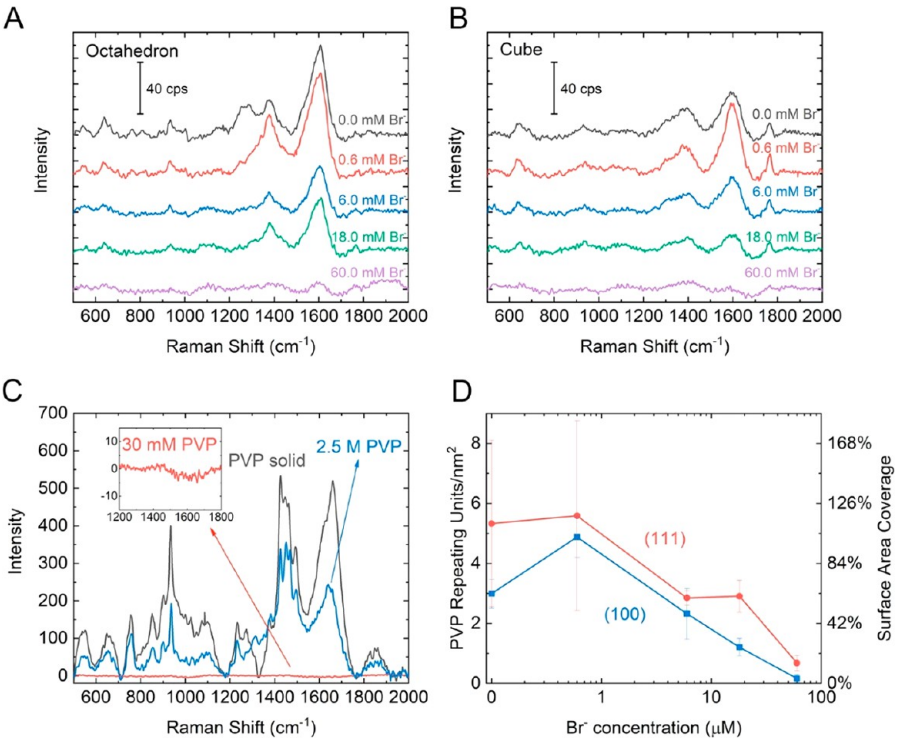

Figure 7. (A, B) SERS spectra of PVP at different Br^- concentrations: (A) in the presence of Ag octahedra and (B) in the presence of Ag cubes. (C) Raman spectra of the PVP solid and solutions. (D) Number of PVP repeating units and their surface area coverage on Ag(100) and Ag(111) at different Br^- concentrations.

worth noting that the addition of 30 mM PVP alone causes approximately 80% passivation for AA oxidation (Figure 5E), indicating that Br^- further passivates AA oxidation in the presence of PVP. These results suggest that AA oxidation is the rate-limiting step for the growth of Ag nanocrystals in the presence of PVP and Br^-. The combined effect of 30 mM PVP and 60 μM Br^- led to 98% passivation of AA oxidation on Ag(100) and 96% on Ag(111) compared with the condition without capping agents (Figure 5F). Given that AA oxidation occurs at a similar rate on Ag(100) and Ag(111) in the absence of capping agents (Figure 4A), such passivation would result in AA oxidation occurring twice as fast on Ag(111) than on Ag(100), as $(1-96\%)j_{(111)}/(1-98\%)j_{(100)} \approx 2$. The strong passivation of AA oxidation significantly reduces the reducing power of AA near Ag surfaces, shifting the E_{mp} to a more positive potential, where Ag^+ reduction occurs at a very slow rate.

We conducted further studies on the effect of Br^- concentration on $j_{mp}^{(100)}$ and $j_{mp}^{(111)}$ (Figure S2). With an increase in Br^- concentration from 0 to 60 μM, $j_{mp}^{(100)}$ decreases, while $j_{mp}^{(111)}$ shows a slight increase at 0.6 μM and then decreases after 6 μM (Figure 6A). In the presence of 30 mM PVP, the addition of 0.6–60 μM Br^- generally leads to a decrease in both $j_{mp}^{(100)}$ and $j_{mp}^{(111)}$ as the Br^- concentration increases (Figure 6B).

It is noteworthy that Br^- consistently exhibits a greater passivation effect on Ag(100) compared to Ag(111) with or without PVP. In the absence of PVP, the R_j value is never smaller than or equal to the R value of 0.58 for cubes (Figure 5C), which aligns with the formation of truncated cubes in the synthesis (Figures 1C and 2B–D). In the presence of PVP, the addition of 0.6 and 6 μM Br^- to 30 mM PVP decreases R_j from 1.16 to 0.65–0.89 (Figure 6D), supporting the formation of truncated cubes with some cuboctahedra (Figure 3B,C). In the presence of 30 mM PVP and 60 μM Br^-, R_j is smaller than the R value of 0.58 for cubes (Figures 4F and 6D), indicating that the growth of nanocubes can happen (Figure 1D).

Adsorption of PVP and Br^- for the Growth of Ag Nanocubes. To investigate the adsorption of PVP and Br^- and understand why Br^- promotes the growth of Ag nanocubes only in the presence of PVP, we employed surface-enhanced Raman spectroscopy (SERS). Two types of Ag nanocrystals, Ag nanocubes covered by the {100} facets and Ag octahedra covered by the {111} facets, were synthesized. The concentrations of these nanocrystals were determined using a dithizone-based colorimetric assay,[34] and their SERS measurements were performed at a concentration of 1.2×10^{11} particles/mL. The enhancement factors (EF) for the nanocubes (0.866×10^4) and octahedra (1.21×10^4) were determined using 1,4-benzenedithiol (1,4-BDT) as a reference molecule, which exhibits non-facet-selective binding on silver and Raman signals.[38] The EF values were used to calculate the surface densities of PVP repeating units on Ag surfaces. Detailed methods are described in the Supporting Information.

Figures 7A and 7B show the SERS spectra of 30 mM PVP at different Br^- concentrations in the presence of Ag nanocubes and octahedra. These spectra exhibit Raman bands similar to those of solid PVP powder and a 2.5 M PVP aqueous solution (Figure 7C). Notably, no Raman signal was detected from an aqueous solution of 30 mM PVP (Figure 7C), indicating that the observed SERS signals exclusively originate from PVP adsorbed on the Ag surface. Because PVP is a polymer, it is possible that only a portion of the PVP chain binds to the Ag surface, while the rest of the chain remains dangling. Previous studies have shown that the SERS intensity dramatically decreases when the distance between the metal surface and the

https://doi.org/10.1021/acs.chemmater.3c01485
Chem. Mater. 2023, 35, 7196–7207

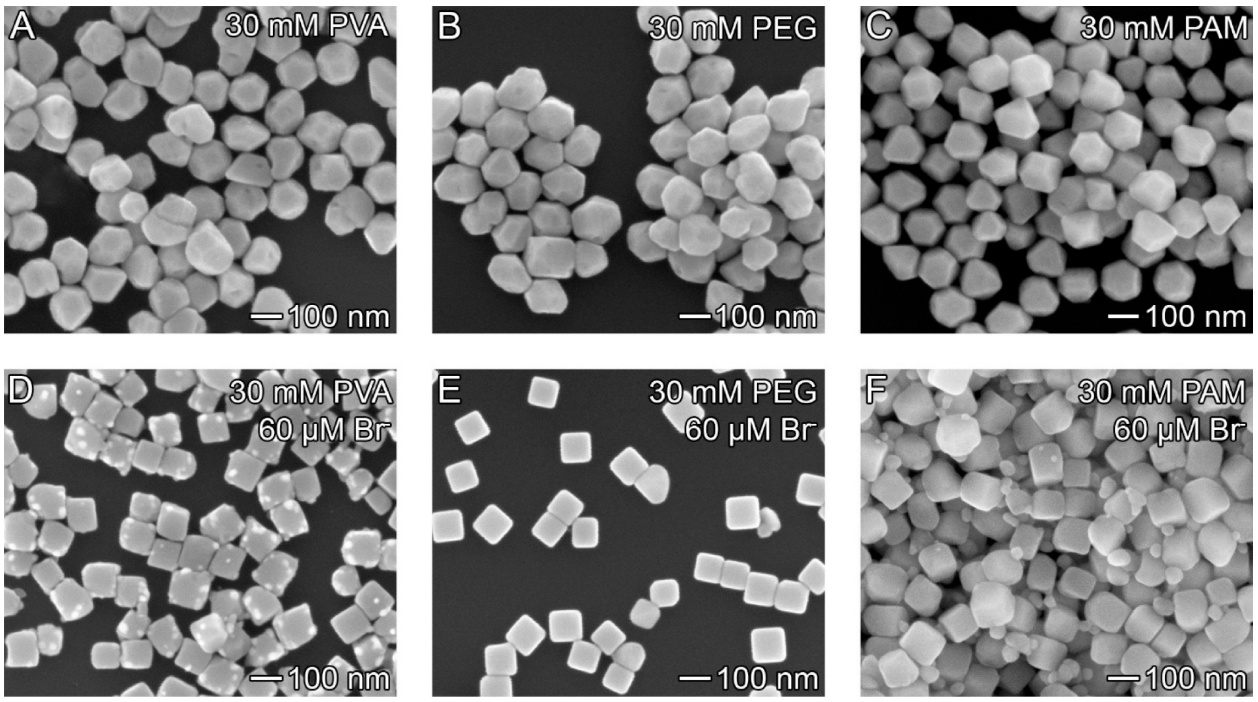

Figure 8. SEM images of silver nanocrystals grown from single-crystal seeds in the presence of different polymers and Br^-: (A) 30 mM PVA, (B) 30 mM PEG, (C) 30 mM PAM, (D) 30 mM PVA and 60 μM Br^-, (E) 30 mM PEG and 60 μM Br^-, and (F) 30 mM PAM and 60 μM Br^-. All seed-mediated growth was performed by using 0.2 mM CF_3COOAg as a silver precursor and 0.4 mM AA as a reducing agent.

analyte increases.[39] This suggests that the majority of the Raman signal arises from the PVP repeating units that directly bind to the Ag surface, while repeating units more than 2 nm away from the surface contribute minimally to the overall Raman signal.

Given that the Raman band at 1600 cm^{-1} exhibits the strongest intensity, the area of this band was used to quantify the surface density of PVP (Figure 7A,B). Because Ag nanocubes are only enclosed by {100} while Ag octahedra are only enclosed by {111}, we were able to measure the surface density of PVP on {100} and {111} facets by separately using one of these two types of nanocrystals for SERS. The SERS spectrum of 30 mM PVP in the presence of 1.2×10^{11}/mL Ag nanocubes has a band area of 2864 at 1600 cm^{-1}, while the Raman spectra of 2.50 M PVP (1.50×10^{21} repeating units/mL) without any Ag nanocrystals have a band area of 24281. The number of PVP repeating units adsorbed on the Ag nanocubes (N_{SERS}) can be calculated by the formula

$$N_{SERS} = N_{bulk}A_{SERS}/(A_{bulk}EF) = 2.04 \times 10^{16} \text{ repeating units/mL}$$

where A_{SERS} is the band area of 30 mM PVP with Ag nanocubes, A_{bulk} is the band area of 2.5 M PVP without Ag nanocrystals, N_{bulk} is the number of PVP repeating units per unit volume in the absence of Ag nanocrystals, and EF is the enhancement factor of Ag nanocrystals. 1.2×10^{11}/mL Ag nanocubes have a total surface area of 6.83×10^{15} nm^2/mL, giving a PVP surface density of 2.99 repeating unites/nm^2.

In the absence of Br^-, the surface density of PVP is 2.99 ± 0.48 repeating units/nm^2 on {100} and 5.33 ± 2.78 repeating units/nm^2 on {111} (Figure 7D). Assuming a monolayer adsorption of PVP and considering that each repeating unit covers approximately 0.21 nm^2 of surface area,[38] the surface area coverage is calculated to be 62.8 ± 10.0% for {100} and 112 ± 58% for {111}. The surface area coverage slightly exceeds 100% due to the weak contribution of dangling PVP repeating units adjacent to the adsorbed ones to the overall SERS signal. These results indicate a higher surface coverage of PVP on {111} compared to that on {100} in the presence of 30 mM PVP, which agrees with the formation of truncated octahedra in the synthesis (Figure 1B).

The surface density of PVP is strongly influenced by the concentration of Br^- (Figure 7D). Addition of 0.6 μM Br^- increases the surface density of PVP by 63.2% to 4.88 ± 0.69 repeating units/nm^2 on {100} and by 4.9% to 5.59 ± 3.16 repeating units/nm^2 on {111}, indicating that a small amount of Br^- primarily enhances the binding of PVP to {100}. Previous studies have demonstrated that Br^- can potentially enhance Raman signals on the Ag surface, and the enhancement becomes stronger at higher Br^- concentrations until saturated.[40,41] However, this mechanism is unlikely to explain the observed rise in Raman intensity of PVP in the presence of 0.6 μM Br^- due to the concurrent decrease in Raman intensity at higher concentrations of Br^- (Figure 7D).[41,42]

When the Br^- concentration is further increased to 6, 18, and 60 μM, the surface density of PVP decreases significantly (Figure 7D). In the presence of 60 μM Br^- where single-crystal seeds grow into cubes, the surface density of PVP is reduced by 95% to 0.16 ± 0.14 repeating units/nm^2 on {100} and by 87% to 0.68 ± 0.27 repeating units/nm^2 on {111}. Such low surface densities of PVP only cover 3.4 ± 2.9% of the surface area of {100} and 14.2 ± 5.6% of the surface area of {111}. These findings demonstrate that Br^- enhances PVP binding at low Br^- concentrations but displaces PVP at high Br^- concentrations. Nevertheless, the surface density of PVP is consistently higher on {111} than on {100} at all Br^- concentrations, suggesting that the growth of cubes at high Br^- concentrations (18−120 μM) is unlikely due to facet-selective binding of PVP.

https://doi.org/10.1021/acs.chemmater.3c01485
Chem. Mater. 2023, 35, 7196−7207

The formation of cubes and the significant displacement of PVP from the Ag surface at high Br^- concentrations indicate that the substantial chemisorption of Br^- on the Ag surface is crucial for the growth of cubes. However, Br^- chemisorption in the absence of PVP does not lead to cube formation, suggesting that PVP still plays an important role in the growth process (Figure 2). Compared with the condition with 60 μM Br^-, the addition of 30 mM PVP and 60 μM Br^- makes $j_{mp}^{(100)}$ decrease by 92.3% from 40.3 to 3.1 $\mu A/cm^2$ and $j_{mp}^{(111)}$ decrease by 87.8% from 57.2 to 7.0 $\mu A/cm^2$ (Figure 4). These substantial decreases in current densities indicate that PVP remains a significant passivator, even though there is very little chemisorption of PVP on the Ag surface. One possible explanation is that PVP is still physisorbed over the Br^- adlayer, with most of the PVP chains dangling far away from the Ag surface. These dangling chains of PVP act as physical barriers, impeding the mass transport of ascorbic acid and resulting in strong but non-facet-selective passivation on both facets. Therefore, we propose that the chemisorption of Br^- beneath the physisorbed layer of PVP on the Ag surface creates a unique condition for the growth of Ag nanocubes.

To investigate the proposed adsorption structure further, the role of PVP as a non-facet-selective physical barrier was examined by replacing it with other polymers. The seed-mediated growth of Ag nanocrystals was performed using various hydrophilic polymers, such as PVA, PEG, and PAM (Figure 8). In the presence of 30 mM PVA, PEG, or PAM, the single-crystal seeds grew into cuboctahedra or truncated octahedra (Figure 8A–C). However, when 60 μM Br^- was added to the solution containing 30 mM PVA or PEG, the single-crystal seeds grew into cubes (Figure 8D,E). In the presence of 30 mM PAM and 60 μM Br^-, the single-crystal seeds grew into truncated cubes (Figure 8F). These results demonstrate that the growth of Ag nanocubes is not unique to PVP but is a general outcome of Br^- adsorption under a wide range of hydrophilic polymers.

It is important to note that a significant number of irregularly shaped particles that are smaller than the seeds were formed when PVA or PAM was combined with Br^- (Figure 8D,F). These observations suggest that polymeric capping agents may play a crucial role in controlling nucleation. In the past two decades, there have been very few successful examples of synthesizing Ag nanocubes in the absence of PVP, which could be attributed to the limited control over nucleation achieved by other polymers.[9,43,44] Further investigation into the roles of polymers in nucleation is essential for achieving precise structure control in colloidal synthesis.

CONCLUSIONS

In this study, a combination of seed-mediated growth, electrochemical measurements, and surface-enhanced Raman spectroscopy (SERS) was employed to investigate the roles of PVP and Br^- in the growth of single-crystal silver nanocrystals. It was found that Br^- acts as a weak capping agent for the {100} facets, as evidenced by an electrochemically measured R_j value of 0.704. This weak capping effect leads to the growth of single-crystal seeds into truncated cubes with an R of 0.69, along with irregular particles. However, when Br^- is added in the presence of PVP, these additives jointly act as strong {100} capping agents. This is reflected in the electrochemically measured R_j value of 0.44, indicating a more effective passivation of the {100} facets. As a result, the single-crystal seeds grow into nanocubes with an R value of 0.58.

SERS spectra provided further insights into how these additives cause the growth of nanocubes. The spectra demonstrated that the presence of 60 μM Br^- almost completely prevents PVP from directly binding to both Ag(100) and Ag(111) surfaces. However, electrochemical measurements indicate that PVP is still physisorbed over the Br^- adlayer. Moreover, it was observed that the presence of Br^- with other hydrophilic polymers also leads to the growth of Ag nanocubes, suggesting that the formation of a chemisorbed Br^- adlayer beneath a physisorbed polymer adlayer is a general adsorption structure for the growth of Ag nanocubes. Overall, this study provides valuable insights into the mechanisms underlying the growth of Ag nanocubes and highlights the critical role of Br^- and hydrophilic polymers in achieving this specific morphology.

ASSOCIATED CONTENT

Supporting Information

The Supporting Information is available free of charge at https://pubs.acs.org/doi/10.1021/acs.chemmater.3c01485.

Determination of Ag nanocube and octahedron concentrations, determination of SERS EFs, schematic representations of different types of nanocrystals, additional LSV measurements, additional Raman measurements, and additional details about experimental measurements (PDF)

AUTHOR INFORMATION

Corresponding Author

Benjamin J. Wiley − *Department of Chemistry, Duke University, Durham, North Carolina 27708, United States;* orcid.org/0000-0002-1314-6223; Email: benjamin.wiley@duke.edu

Authors

Heng Xu − *Department of Chemistry, Duke University, Durham, North Carolina 27708, United States;* orcid.org/0000-0002-8259-5516

Spencer Hao − *Department of Chemistry, Duke University, Durham, North Carolina 27708, United States;* orcid.org/0000-0003-4463-0138

Complete contact information is available at: https://pubs.acs.org/10.1021/acs.chemmater.3c01485

Notes

The authors declare no competing financial interest.

ACKNOWLEDGMENTS

This work was supported by NSF Grant CHE-1808108. SEM, Raman, and UV–vis–NIR spectroscopy were performed at the Duke University Shared Materials Instrumentation Facility (SMIF), a member of the North Carolina Research Triangle Nanotechnology Network (RTNN), which is supported by the National Science Foundation (Award No. ECCS-2025064) as part of the National Nanotechnology Coordinated Infrastructure (NNCI).

REFERENCES

(1) Kuo, T.-R.; Lee, Y.-C.; Chou, H.-L.; M G, S.; Wei, C.-Y.; Wen, C.-Y.; Chang, Y.-H.; Pan, X.-Y.; Wang, D.-Y. Plasmon-Enhanced

Hydrogen Evolution on Specific Facet of Silver Nanocrystals. *Chem. Mater.* **2019**, *31*, 3722−3728.
(2) Scarabelli, L.; Sun, M.; Zhuo, X.; Yoo, S.; Millstone, J. E.; Jones, M. R.; Liz-Marzán, L. M. Plate-Like Colloidal Metal Nanoparticles. *Chem. Rev.* **2023**, *123*, 3493−3542.
(3) Zheng, J.; Cheng, X.; Zhang, H.; Bai, X.; Ai, R.; Shao, L.; Wang, J. Gold Nanorods: The Most Versatile Plasmonic Nanoparticles. *Chem. Rev.* **2021**, *121*, 13342−13453.
(4) Hsieh, C.-J.; Liu, Y.-H.; Tsao, C.-Y.; Lin, J.-T.; Chi, C.-C.; Chang, C.-W.; Hsiao, Y.-C.; Wu, C.-Y.; Yang, T.-H. Bromide-Mediated Reduction Kinetics and Oxidative Etching for Manipulating the Twin Structure and Facet of Pd Nanocrystals for Catalysis. *Adv. Mater. Interfaces* **2022**, *9*, No. 2201036.
(5) De Gregorio, G. L.; Burdyny, T.; Loiudice, A.; Iyengar, P.; Smith, W. A.; Buonsanti, R. Facet-Dependent Selectivity of Cu Catalysts in Electrochemical CO_2 Reduction at Commercially Viable Current Densities. *ACS Catal.* **2020**, *10*, 4854−4862.
(6) Shi, Y.; Lyu, Z.; Zhao, M.; Chen, R.; Nguyen, Q. N.; Xia, Y. Noble-Metal Nanocrystals with Controlled Shapes for Catalytic and Electrocatalytic Applications. *Chem. Rev.* **2021**, *121*, 649−735.
(7) Li, Z.; Fu, J.-Y.; Feng, Y.; Dong, C.-K.; Liu, H.; Du, X.-W. A silver catalyst activated by stacking faults for the hydrogen evolution reaction. *Nat. Catal.* **2019**, *2*, 1107−1114.
(8) Kim, M.; Lee, J.-H.; Nam, J.-M. Plasmonic Photothermal Nanoparticles for Biomedical Applications. *Adv. Sci.* **2019**, *6*, No. 1900471.
(9) Yang, T.-H.; Shi, Y.; Janssen, A.; Xia, Y. Surface Capping Agents and Their Roles in Shape-Controlled Synthesis of Colloidal Metal Nanocrystals. *Angew. Chem., Int. Ed.* **2020**, *59*, 15378−15401.
(10) Chen, Z.; Balankura, T.; Fichthorn, K. A.; Rioux, R. M. Revisiting the Polyol Synthesis of Silver Nanostructures: Role of Chloride in Nanocube Formation. *ACS Nano* **2019**, *13*, 1849−1860.
(11) Brown, M.; Wiley, B. J. Bromide Causes Facet-Selective Atomic Addition in Gold Nanorod Syntheses. *Chem. Mater.* **2020**, *32*, 6410−6415.
(12) Fichthorn, K. A. Theory of Anisotropic Metal Nanostructures. *Chem. Rev.* **2023**, *123*, 4146−4183.
(13) Kim, M. J.; Alvarez, S.; Chen, Z.; Fichthorn, K. A.; Wiley, B. J. Single-Crystal Electrochemistry Reveals Why Metal Nanowires Grow. *J. Am. Chem. Soc.* **2018**, *140*, 14740−14746.
(14) Zeng, J.; Xia, X.; Rycenga, M.; Henneghan, P.; Li, Q.; Xia, Y. Successive Deposition of Silver on Silver Nanoplates: Lateral versus Vertical Growth. *Angew. Chem., Int. Ed.* **2011**, *50*, 244−249.
(15) Zhang, Q.; Li, N.; Goebl, J.; Lu, Z.; Yin, Y. A Systematic Study of the Synthesis of Silver Nanoplates: Is Citrate a "Magic" Reagent? *J. Am. Chem. Soc.* **2011**, *133*, 18931−18939.
(16) Wang, Y.; Wan, D.; Xie, S.; Xia, X.; Huang, C. Z.; Xia, Y. Synthesis of Silver Octahedra with Controlled Sizes and Optical Properties via Seed-Mediated Growth. *ACS Nano* **2013**, *7*, 4586−4594.
(17) Lin, Z.-W.; Tsao, Y.-C.; Yang, M.-Y.; Huang, M. H. Seed-Mediated Growth of Silver Nanocubes in Aqueous Solution with Tunable Size and Their Conversion to Au Nanocages with Efficient Photothermal Property. *Chem.—Eur. J.* **2016**, *22*, 2326−2332.
(18) Yu, D.; Yam, V. W.-W. Controlled Synthesis of Monodisperse Silver Nanocubes in Water. *J. Am. Chem. Soc.* **2004**, *126*, 13200−13201.
(19) Ruditskiy, A.; Xia, Y. Toward the Synthesis of Sub-15 nm Ag Nanocubes with Sharp Corners and Edges: The Roles of Heterogeneous Nucleation and Surface Capping. *J. Am. Chem. Soc.* **2016**, *138*, 3161−3167.
(20) Fan, Z.; Chen, J.; Mao, H.; Yin, J.; Dai, W.; He, L.; Yang, H. Synthesis and the growth mechanism of ultrafine silver nanowires by using 5-chloro-2-thienylmagnesium bromide as the additive. *RSC Adv.* **2021**, *11*, 37063−37066.
(21) Yuan, X.; Yang, H.; Li, Y.; Chao, Y.; Li, Y.; Chen, L.; Chen, J. A novel synthesis of silver nanowires by using 6-chlorohexylzinc bromide as an additive for low haze transparent conductive films. *RSC Adv.* **2019**, *9*, 18868−18873.
(22) Li, B.; Ye, S.; Stewart, I. E.; Alvarez, S.; Wiley, B. J. Synthesis and Purification of Silver Nanowires To Make Conducting Films with a Transmittance of 99%. *Nano Lett.* **2015**, *15*, 6722−6726.
(23) da Silva, R. R.; Yang, M.; Choi, S.-I.; Chi, M.; Luo, M.; Zhang, C.; Li, Z.-Y.; Camargo, P. H. C.; Ribeiro, S. J. L.; Xia, Y. Facile Synthesis of Sub-20 nm Silver Nanowires through a Bromide-Mediated Polyol Method. *ACS Nano* **2016**, *10*, 7892−7900.
(24) Niu, Z.; Cui, F.; Kuttner, E.; Xie, C.; Chen, H.; Sun, Y.; Dehestani, A.; Schierle-Arndt, K.; Yang, P. Synthesis of Silver Nanowires with Reduced Diameters Using Benzoin-Derived Radicals to Make Transparent Conductors with High Transparency and Low Haze. *Nano Lett.* **2018**, *18*, 5329−5334.
(25) Orendorff, C. J.; Gearheart, L.; Jana, N. R.; Murphy, C. J. Aspect ratio dependence on surface enhanced Raman scattering using silver and gold nanorod substrates. *Phys. Chem. Chem. Phys.* **2006**, *8*, 165−170.
(26) Wiley, B. J.; Chen, Y.; McLellan, J. M.; Xiong, Y.; Li, Z.-Y.; Ginger, D.; Xia, Y. Synthesis and Optical Properties of Silver Nanobars and Nanorice. *Nano Lett.* **2007**, *7*, 1032−1036.
(27) Wiley, B. J.; Xiong, Y.; Li, Z.-Y.; Yin, Y.; Xia, Y. Right Bipyramids of Silver: A New Shape Derived from Single Twinned Seeds. *Nano Lett.* **2006**, *6*, 765−768.
(28) Chen, S.; Carroll, D. L. Silver Nanoplates: Size Control in Two Dimensions and Formation Mechanisms. *J. Phys. Chem. B* **2004**, *108*, 5500−5506.
(29) Chen, S.; Carroll, D. L. Synthesis and Characterization of Truncated Triangular Silver Nanoplates. *Nano Lett.* **2002**, *2*, 1003−1007.
(30) Lee, B.-H.; Hsu, M.-S.; Hsu, Y.-C.; Lo, C.-W.; Huang, C.-L. A Facile Method To Obtain Highly Stable Silver Nanoplate Colloids with Desired Surface Plasmon Resonance Wavelengths. *J. Phys. Chem. C* **2010**, *114*, 6222−6227.
(31) Tang, B.; Xu, S.; An, J.; Zhao, B.; Xu, W.; Lombardi, J. R. Kinetic effects of halide ions on the morphological evolution of silver nanoplates. *Phys. Chem. Chem. Phys.* **2009**, *11*, 10286−10292.
(32) Xu, H.; Wiley, B. J. The Roles of Citrate and Defects in the Anisotropic Growth of Ag Nanostructures. *Chem. Mater.* **2021**, *33*, 8301−8311.
(33) Wiley, B.; Sun, Y.; Xia, Y. Polyol Synthesis of Silver Nanostructures: Control of Product Morphology with Fe(II) or Fe(III) Species. *Langmuir* **2005**, *21*, 8077−8080.
(34) Wasukan, N.; Srisung, S.; Kuno, M.; Kulthong, K.; Maniratanachote, R. Interaction evaluation of silver and dithizone complexes using DFT calculations and NMR analysis. *Spectrochim. Acta A Mol. Biomol. Spectrosc.* **2015**, *149*, 830−838.
(35) Sun, Y. G.; Xia, Y. N. Shape-controlled synthesis of gold and silver nanoparticles. *Science* **2002**, *298*, 2176−2179.
(36) Wang, Z. L. Transmission Electron Microscopy of Shape-Controlled Nanocrystals and Their Assemblies. *J. Phys. Chem. B* **2000**, *104*, 1153−1175.
(37) Xu, H.; Chen, Z.; Hao, S.; Fichthorn, K. A.; Wiley, B. J. Chloride enables the growth of Ag nanocubes and nanowires by making PVP binding facet-selective. *Nanoscale* **2023**, *15*, 5219−5229.
(38) Xia, X.; Zeng, J.; Oetjen, L. K.; Li, Q.; Xia, Y. Quantitative Analysis of the Role Played by Poly(vinylpyrrolidone) in Seed-Mediated Growth of Ag Nanocrystals. *J. Am. Chem. Soc.* **2012**, *134*, 1793−1801.
(39) Li, J. F.; Huang, Y. F.; Ding, Y.; Yang, Z. L.; Li, S. B.; Zhou, X. S.; Fan, F. R.; Zhang, W.; Zhou, Z. Y.; Wu, D. Y.; et al. Shell-isolated nanoparticle-enhanced Raman spectroscopy. *Nature* **2010**, *464*, 392−395.
(40) Doering, W. E.; Nie, S. Single-Molecule and Single-Nanoparticle SERS: Examining the Roles of Surface Active Sites and Chemical Enhancement. *J. Phys. Chem. B* **2002**, *106*, 311−317.
(41) Hildebrandt, P.; Stockburger, M. Surface-enhanced resonance Raman spectroscopy of Rhodamine 6G adsorbed on colloidal silver. *J. Phys. Chem.* **1984**, *88*, 5935−5944.

https://doi.org/10.1021/acs.chemmater.3c01485
Chem. Mater. 2023, 35, 7196−7207

(42) Otto, A.; Mrozek, I.; Grabhorn, H.; Akemann, W. SURFACE-ENHANCED RAMAN-SCATTERING. *J. Phys.: Condens. Matter* **1992**, *4*, 1143−1212.
(43) Zhou, S.; Li, J.; Gilroy, K. D.; Tao, J.; Zhu, C.; Yang, X.; Sun, X.; Xia, Y. Facile Synthesis of Silver Nanocubes with Sharp Corners and Edges in an Aqueous Solution. *ACS Nano* **2016**, *10*, 9861−9870.
(44) Pawlik, V.; Zhou, S.; Zhou, S.; Qin, D.; Xia, Y. Silver Nanocubes: From Serendipity to Mechanistic Understanding, Rational Synthesis, and Niche Applications. *Chem. Mater.* **2023**, *35*, 3427−3449.

https://doi.org/10.1021/acs.chemmater.3c01485
Chem. Mater. 2023, 35, 7196−7207